

Date of publication xxxx 00, 0000, date of current version xxxx 00, 0000.

Digital Object Identifier

Efficient Design Procedure for Comblines Bandpass Filters with Advanced Electrical Responses

HOJJAT JAMSHIDI-ZARMEHRI¹, ÁNGEL A. SAN-BLAS², MOHAMMAD H. NESHATI¹, (Senior Member, IEEE), SANTIAGO COGOLLOS³, (Member, IEEE), ABHISHEK SHARMA³, VICENTE E. BORJA³, (Fellow, IEEE), AND ÁNGELA COVES², (Senior Member, IEEE)

¹Electrical Engineering Department, Ferdowsi University of Mashhad, 91779-48974 Mashhad, Iran (e-mail: jamshidi68hojat@gmail.com, neshat@um.ac.ir)

²Department of Communications Engineering-I3E, Miguel Hernández University of Elche, 03202 Elche, Spain (e-mail: aasanblas@umh.es, angela.coves@umh.es)

³iTEAM Group, Departamento de Comunicaciones, Universitat Politècnica de València, 46022 Valencia, Spain (e-mail: sancobo@dcom.upv.es, asharma@iteam.upv.es, vborja@dcom.upv.es)

Corresponding author: A. A. San-Blas (e-mail: aasanblas@umh.es).

This work was supported by the Ministerio de Ciencia e Innovación, Spanish Government, through the Subprojects C43 and C41 of the Coordinated Research and Development Projects PID2019-103982RB and TED2021-129196B, under Grant MCIN/AEI/10.13039/501100011033, and also by Conselleria d'Innovació, Universitats, Ciència i Societat Digital, Generalitat Valenciana (Project CIAICO/2021/055).

ABSTRACT In this paper, a very efficient procedure for designing waveguide comblines bandpass filters with an advanced electrical response is presented. The proposed technique is based on a segmentation strategy, which reduces the number of variables to be optimized by dividing the design process into simpler stages. The electrical response of an appropriate equivalent circuit model of the waveguide structure considered in each stage is used to generate the target curve needed in the optimization process. Moreover, the well-known Aggressive Space Mapping technique has been also implemented to improve the computational efficiency of the whole method. In order to validate the proposed design procedure, two high-order comblines bandpass filters, with symmetric and asymmetric electrical responses including transmission zeros, have been successfully designed and simulated with full-wave analysis tools. Furthermore, as an experimental validation, a prototype of the symmetric filter has been manufactured, showing a good agreement between simulated and experimental data.

INDEX TERMS Aggressive space mapping, bandpass filters, comblines filters, coupling matrix, cul-de-sac filter, equivalent circuit model.

I. INTRODUCTION

Microwave bandpass filters have a wide range of applications in satellite and wireless communications systems, and they can be implemented using different topologies and technologies. The most appropriate realization technique is usually selected based on the required electrical specifications, and also on the different system requirements and constraints [1]. In this context, waveguide comblines filters represent a class of bandpass filters that exhibits some important advantages, such as a high degree of compactness and a good power handling capability [2], [3]. Although comblines filters are typically implemented using rectangular cavities loaded with cylindrical metal posts [4], other non-canonical topologies have also been investigated in the past, as the new family

of comblines filters based on triangular resonators recently presented in [5], or the inline configuration outlined in [6], where the resonator posts are transversally positioned and mutually rotated in a circularly shaped cavity.

In this type of waveguide filters, rectangular irises are frequently used to implement either magnetic or electric couplings between resonators. The height and the position of the coupling windows determine the amount and the sign of the coupling coefficient [4]. Besides, although comblines filters are classically implemented using an inline configuration [7], [8], [9] (metal and dielectric tuners can also be employed for reconfigurability purposes, as in [10], [11]), folded arrangements are preferred if the filter selectivity needs to be enhanced by the implementation of transmission zeros (TZs)

[2], [4], [12], [13], [14]. However, TZs can also be realized using an inline configuration. For instance, inline combine filters employing resonators loaded with planar rectangular posts have been recently investigated in [15], where several bandpass filters exhibiting TZs below and above the passband have been designed and fabricated using printed circuit board (PCB) technology. In this solution, the practical implementation of physical structures providing mixed inductive and capacitive couplings is required. Another example of an inline topology with TZs can be found in [16], where the different resonator posts alternate their position to introduce several cross-couplings. Yet another interesting approach was presented in [17], where the three coaxial resonators of the designed tunable filter are arranged in a triangle shape. More recently, extracted-pole filters using non-resonant nodes have been investigated in [18]. In that work, an inline combine filter providing two TZs in the upper side of the passband has been designed, using mapping relationships between the coupling matrix elements and the dimensions of the real filter.

Other coupling topologies, such as the so-called cul-de-sac and box-section configurations, can also be employed to implement TZs placed on both the upper and lower sides of the passband [19]–[22]. Advanced filter responses using the cul-de-sac configuration were initially proposed in [19], [21]. Using this topology, asymmetric electrical responses can be synthesized without resorting to diagonal cross-couplings, thus overcoming different problems that may arise during the manufacture of a prototype.

Next, it would be worth discussing the results of our review of previous relevant contributions in the context of bandpass filters design. The design of a filter typically starts with a set of given electrical specifications. Afterwards, the well-established approach consists of deriving an appropriate coupling matrix that fulfils the specifications [2], [23]. Other works rely instead on the obtention of an equivalent circuit model in terms of lumped elements and inverters, as in [7], [16], [18].

The resonant frequencies of the cavities and the input/output couplings are first modelled and, afterwards, the inter-resonator couplings are considered. After completing these steps, an initial set of filter dimensions is obtained and, finally, the whole filter is assembled. The initial electrical response of the filter is then compared with the response provided by the derived coupling matrix (or by the equivalent circuit model) and, by means of a full-wave simulator, the dimensions of the physical structure are iteratively optimized until the desired electrical response is recovered [4], [6], [11], [13], [14], [17], [18], [24]. Proceeding in this way, however, the complete set of the filter dimensions is optimized at the same time. Therefore, if a complex high-order filter needs to be designed, the number of involved physical dimensions will increase, and the optimization algorithm employed to adjust the design variables will typically require high CPU resources. In some cases, the optimization algorithm can even get trapped in a local minimum when a large number of design variables are handled.

In contrast to the aforementioned classical design technique, the reflected group delay method (firstly introduced by Ness in [25]) proposed a segmentation of the structure to divide the design process into simpler stages, with the aim of decreasing the number of optimized variables in each step of the procedure. Ness' technique has been successfully used for the design of several bandpass filters implemented in different technologies [26], [27], [28]. Moreover, a very efficient design technique, combining a segmentation of the structure and the use of a circuit model based on lumped elements and ideal impedance inverters, was presented in [29] for designing low-order rectangular waveguide combine filters in a folded configuration (without including TZs). A similar strategy was followed in [30] for the design of compact H-plane (inductive) rectangular waveguide filters including a coaxial excitation.

However, in our review of the technical literature, very few works deal with the efficient design of high-order waveguide combine filters with advanced electrical responses, reporting detailed guidelines for the determination of all the physical dimensions of the designed structure (this is, in fact, one of the main contributions of the present work). The only relevant work we have found is [12], where a step-by-step design procedure based on the obtention of an appropriate input impedance phase was presented. Although a waveguide combine filter with two TZs was designed in that work, the considered structure was a low-order filter (fourth-order) with a classical folded arrangement, providing a symmetric frequency response. Another relevant work that is worth to be cited is [19], where several waveguide combine filters in a cul-de-sac configuration were successfully designed and manufactured. However, the design guidelines followed to achieve the real physical dimensions of the synthesized filters were not detailed. Furthermore, different design guidelines have been reported in [2] with the aim of characterizing some dimensions (e.g. inter-resonator and input/output couplings) of a general filter, and particularly of classical combine configurations. Nevertheless, the design of more complex topologies (as the aforementioned cul-the-sac configuration) is not a straightforward procedure.

In this context, therefore, the main objective of this novel contribution is to present a systematic design procedure, inspired by the segmentation approach (used in [29] and [30] with simple structures), of more complex waveguide combine filters with advanced electrical responses, including cul-de-sac configurations, as the one shown in Fig. 1. Compared to previous contributions on this topic, this novel work provides detailed design guidelines to efficiently obtain the physical dimensions of high-order bandpass filters (with symmetric and asymmetric frequency responses) implemented in rectangular waveguide combine technology. With the aim of getting responses with TZs located below and above the filter passband, the designed solutions include both electric- and magnetic-type cross-couplings.

The design technique that we propose is based on a proper segmentation of the considered filter structure, and on the

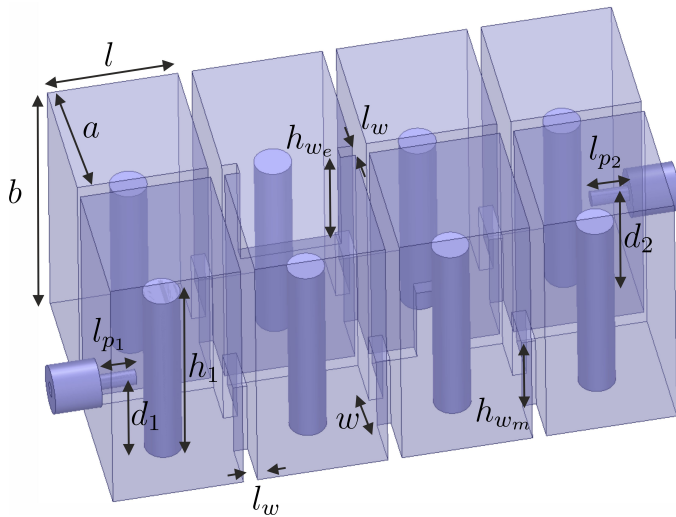


FIGURE 1. Eighth-degree waveguide combline filter in a cul-de-sac configuration.

use of equivalent circuit models. In every design stage, only a section of the combline filter is optimized, by using the group delay of the S_{11} -parameter response of the circuit model of such filter section as the design goal. Proceeding in this way, the different dimensions of the structure are added progressively and, in every step, only few new dimensions are optimized, with the aim of improving the computational efficiency of the design method. This procedure not only reduces the complexity of the design process, but also improves its convergence to the optimal solution. Besides, since the Aggressive Space Mapping (ASM) technique has been used [31], most of the simulations carried out during the optimization process are run in a low-accuracy full-wave electromagnetic (EM) simulation tool, thus drastically reducing the overall CPU time and memory costs. This is one of the main innovative contributions of this work.

Apart from verifying the proposed technique with accurate full-wave simulations, a filter prototype of an 8-th order generalized Chebyshev bandpass filter with 4 TZs operating in the S-band ($f_0 = 3$ GHz) has been manufactured as an experimental validation.

This paper has been organized as follows. Section II details the main steps of the proposed design process. To verify this novel procedure, two high-order combline bandpass filters with advanced electrical responses (both symmetric and asymmetric), and including TZs to improve the response selectivity, are discussed in Section III. For validation purposes, the results of the cul-de-sac combline filter obtained using two accurate full-wave simulation tools, are also successfully compared. Next, section IV details the practical implementation of the designed filter with symmetric response, obtaining a very good agreement between simulated and experimental data. Finally, the main conclusions of this work are summarized in Section V.

II. DESIGN PROCEDURE

In this section, the procedure used to determine the physical dimensions of waveguide combline filters with advanced electrical responses is explained in detail. The designed filters will consist of rectangular cavities loaded with cylindrical posts located in a centered position. The different resonators, that will be arranged in a folded configuration, will be coupled using rectangular windows designed to provide either electric- or magnetic-type couplings, as described in [4]. The designed filters will be excited using a coaxial waveguide, whose inner probe will not be in contact with the resonator metal posts (see Fig. 1).

The proposed design technique consists in a step-by-step procedure, where the different filter resonators are progressively added one after another, with the aim of reducing the number of variables to optimize in each stage. The electrical response of a circuit model of the structure employed in each stage, will be considered as the target response in the optimization process.

A. DESIGN OF THE RESONATOR AND DERIVATION OF ITS EQUIVALENT LUMPED ELEMENTS

In the first step, the dimensions of a rectangular cavity loaded with a cylindrical post should be determined to resonate at the desired frequency f_0 (i.e., the central frequency of the passband). To obtain the relevant dimensions (width, height and length of the resonator, as well as the height and diameter of the post), the eigenmode solver of Ansys HFSS can be used following the guidelines described in [32]. After that, an equivalent circuit of the resonator in terms of a series combination of an inductance and a capacitance (LC series network) should be obtained. To this aim, first, the slope parameter \mathcal{X} of the resonator can be calculated as follows:

$$\mathcal{X} = \frac{\omega_0}{2} \left. \frac{dX_{in}(\omega)}{d\omega} \right|_{\omega=\omega_0} \quad (1)$$

where $\omega_0 = 2\pi f_0$, X_{in} represents the reactance of the input impedance of the cavity, and the derivative of X_{in} must be evaluated at $\omega = \omega_0$. The reactance X_{in} is obtained using Ansys HFSS, by considering a one-port structure obtained after opening the bottom surface of the resonator [32]. Since \mathcal{X} is also equal to $L\omega_0$, the inductance L can be readily obtained. Afterwards, the capacitance C can be calculated as $C = 1/(\omega_0^2 L)$.

It is worth noting that, when designing asymmetric filters, the different resonators are asynchronously tuned, so a frequency-independent reactance (FIR) should be considered in the equivalent circuit of the resonator [2], as shown in Fig. 2. In the next steps of the design process, all the dimensions derived in this stage (except for the height of the post) will not be optimized.

B. OBTENTION OF THE EQUIVALENT CIRCUIT OF THE FILTER

Once the resonators of the filter have been characterized in terms of lumped elements, the next step consists in obtaining

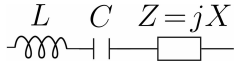


FIGURE 2. Equivalent circuit of the resonator including a frequency-independent reactance $Z = jX$ ($X = 0$ for symmetric filters).

an equivalent circuit of the whole filter. For filters with a symmetric frequency response, the circuit model will be based on ideal impedance inverters (that model the coupling windows of the real filter), and LC series networks representing the resonators. Furthermore, as previously discussed, FIRs must be also included in the circuit model if the filter response is asymmetric. Fig. 3 displays the equivalent circuit of the connection of two resonators using an ideal impedance inverter.

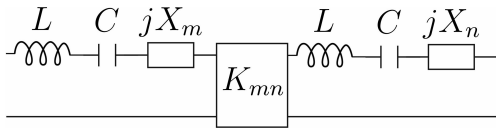


FIGURE 3. Equivalent circuit of the connection of the m -th and n -th resonators.

Given a set of electrical specifications (in terms of f_0 , the prescribed return losses, the order N of the filter, its bandwidth and the number and position of the TZs), the corresponding $N + 2$ coupling matrix is synthesized according to the desired filter configuration and electrical response (cul-de-sac configuration, symmetric or asymmetric filtering response, etc.) [2], [19]. The values K_{ij} of the impedance inverters are obtained starting from the derived coupling matrix elements, by taking into account the effect of the source and the load impedance Z_0 , the bandwidth BW of the filter and the values of the lumped elements (L) of the involved resonators, as follows:

$$K_{ij} = M_{ij} \frac{L}{L_0}, i \neq j \quad (2)$$

$$K_{S1} = K_{NL} = M_{S1} \sqrt{\frac{Z_0 L}{L_0}} \quad (3)$$

where M_{ij} represents the corresponding coupling matrix value, subscripts S and L stand for source and load, respectively, $L_0 = 1/(2\pi BW)$ and $i, j = 1, 2, \dots, N$. Finally, the values of the FIRs can be deduced from the diagonal elements of the coupling matrix, as follows [2]:

$$X_i = M_{ii} \frac{L}{L_0} \quad (4)$$

C. DESIGN OF THE COAXIAL EXCITATION

Comblin filters are two-port components that are frequently fed using coaxial probes [4], [10], [11], [14], [17]. In this section, therefore, the objective is to describe the procedure to derive the initial dimensions related to the coaxial excitation. To this aim, a one-port structure is considered in this step of the design process, consisting in a rectangular cavity

loaded with a cylindrical post and fed by a coaxial probe, as it can be seen in Fig. 4.

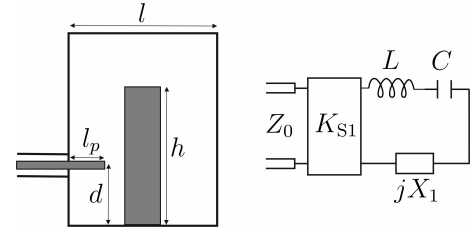


FIGURE 4. Waveguide component used for the design of the coaxial excitation (left) and the corresponding equivalent circuit (right).

The target response is extracted from the equivalent circuit model of the physical component (see Fig. 4, right), which consists of the impedance inverter K_{S1} representing the input/output coupling (its value has been deduced in the previous stage), an LC series network representing the resonator, and a FIR of value jX_1 (to be included only for asymmetric filters). Next, the waveguide structure is optimized (in terms of the group delay of the S_{11} parameter) using an efficient full-wave EM simulation tool (in this case, the commercial software FEST3D), with the aim of obtaining the same electrical response as the circuit model. The dimensions to optimize in this step are (see Fig. 4, left): the height of the resonator loading post (h), the position of the coaxial feeding line (d), and the penetration depth of the coaxial probes (l_p).

D. INITIAL DIMENSIONS OF THE RECTANGULAR COUPLING WINDOWS

Filter resonators are coupled using rectangular waveguide windows that, depending on their location, can implement both electric- and magnetic-type couplings. Usually, magnetic couplings can be achieved by placing the iris at the short-circuit location of the filter resonator, whereas an electric coupling requires to place the iris at the open end of the resonator [4]. In this work, the thickness l_w of all coupling windows (see Fig. 1) is set to 1.5 mm, and this value is not optimized during the design process. It is worth noting that it is better to maintain constant this dimension in order to facilitate the manufacturing process. The chosen value for the thickness (1.5 mm in this work) is able to provide us with the couplings values required by the equivalent circuit models.

First of all, the case of symmetric filters is addressed. With the aim of finding an initial value for the height of electric- and magnetic-type coupling windows (denoted as h_{we} and h_{wm} , respectively, in Fig. 1), 2-port symmetric structures composed of two resonators excited using coaxial lines and coupled through the corresponding rectangular iris are considered (the dimensions related to the resonators and the coaxial excitation have been obtained in the previous design steps). More details on the considered geometries for magnetic-type windows can be found in [29], while the waveguide component to be considered for electric-type coupling windows in folded arrangements is shown in Fig. 5.

After that, the ideal network of the waveguide component is derived (using impedance inverters and LC series networks), and its electrical response in terms of the S_{21} parameter is used as a target. Then, the dimensions of the waveguide structure are optimized in order to get a match with the target response. With the aim of reducing the number of variables to optimize, only the window requiring the strongest coupling is designed following this procedure, and the obtained value of the height is considered as the solution for all the windows of the filter (note that electric and magnetic windows are treated separately, so a different initial height is found in each case).

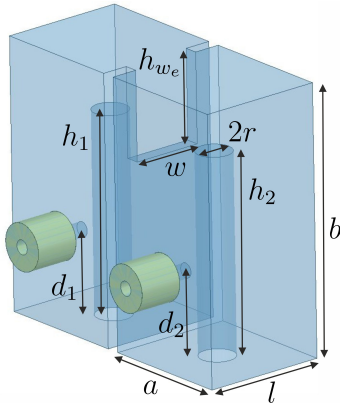


FIGURE 5. Waveguide component used for obtaining the initial dimensions of an electric-type coupling iris.

On the other hand, to obtain an initial value for the widths of the windows (represented as w in Fig. 5), the resonant frequencies of the previously cited 2-port symmetric structures should be determined. For this purpose, as explained in [29], the two involved resonators must be weakly coupled to the input and output coaxial ports (which can be easily achieved in Fig. 5 by properly reducing the length of the coupling coaxial probes). Next, the inter-resonator coupling of these waveguide structures can be readily obtained (in terms of the cited resonant frequencies [2]) as a function of the width of the considered window. Finally, the values for the widths of the coupling windows required to provide the corresponding coupling coefficients k_{ij} of the equivalent circuit ($k_{ij} = K_{ij}/\mathcal{X}$) are initially estimated.

Although this design procedure holds, as well, for filters with an asymmetric frequency response, some relevant changes have to be considered. First of all, FIRs must be taken into account in the corresponding circuit models. For instance, Fig. 6 shows the equivalent circuit of the waveguide component displayed in Fig. 5 for the case of asymmetric filters. Besides, since the filter resonators are asynchronously tuned, 2-port asymmetric structures (instead of symmetric ones) must be used to determine the initial dimensions of the windows. This can be easily achieved in Fig. 5 by using slightly different post heights to account for the differences among the resonant frequencies (which can be evaluated using the values of L , C and X_m of the circuit model resonators).

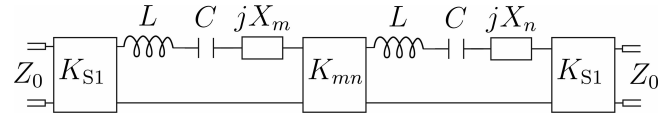


FIGURE 6. Circuit model of the waveguide component in Fig. 5 for the case of asymmetric filters.

In addition, in order to obtain an initial value for the widths of the coupling windows, the inter-resonator coupling coefficient of these asymmetric waveguide structures should be calculated (for each considered window width) using the method and expressions found in [33], in terms of the electric and magnetic resonant frequencies f_e and f_m . Furthermore, the required coupling coefficient of the corresponding equivalent circuit needs to be evaluated, as well. To this end, we propose to use the circuit model of the considered waveguide structure (as the one shown in Fig. 6) by choosing a very low value for the input/output inverter K_{S1} . In order to validate this procedure, Fig. 7 shows the magnitude (in dB) of the S_{21} parameter of the waveguide component in Fig. 5 when the input/output resonators are weakly coupled to the input/output coaxial ports. The electrical response of the related equivalent circuit is also displayed in Fig. 7. It is worth noting that both curves can provide the same values for the inter-resonator coupling coefficient (since their peaks are located at the same frequency points), so this technique is used to obtain the initial dimensions of the electric-type coupling window.

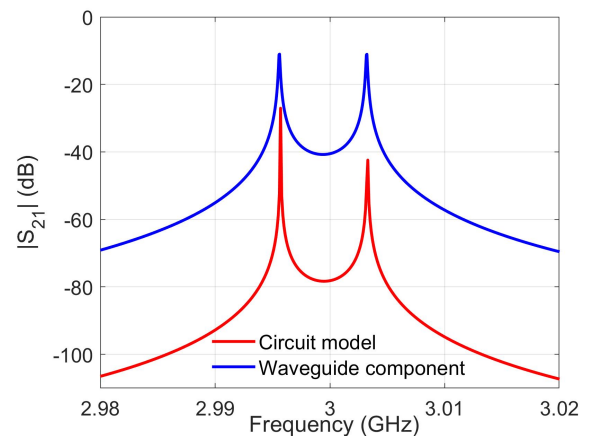


FIGURE 7. Electrical response of the waveguide component of Fig. 5 compared to the response of its circuit model, considering input/output resonators weakly coupled to the coaxial access ports. The dimensions (all in mm) of the waveguide structure (see Fig. 5) are: $a = 15$, $b = 30$, $l = 14$, $h_1 = 22.454$, $h_2 = 22.514$, $r = 2$, $h_{we} = 10$, $w = 7$, $d_1 = 10.247$, $d_2 = 10.251$.

E. ADDITION OF THE RESONATORS OF THE FILTER

In this step of the design process, the filter resonators are added progressively one after the other. The waveguide structure dimensions found in the previous steps are considered as

initial values of each new optimization stage, in order to guarantee the convergence of the design method. In each stage, an equivalent circuit model of the corresponding real structure is obtained, following the guidelines given in Section II-B. Next, the dimensions of the physical structure considered in each stage are optimized by taking the group delay of the S_{11} parameter of the equivalent circuit model as the target response.

For the sake of efficiency, the height of the magnetic-type coupling windows is not optimized in this stage, so that the initial value found in the previous design step is not modified. However, the height of windows implementing an electric coupling may need a further optimization in order to recover the required response, since the value of this type of coupling is more sensitive to the window dimensions. On the other hand, the width of the (electric and magnetic) coupling windows do need to be optimized as the different resonators are progressively added. Regarding the resonator dimensions, only the heights of the loading posts are optimized. Furthermore, all dimensions related to the coaxial excitation of the structure, also need to be re-optimized in this stage of the design process.

More details of this design process stage are given for the two filter examples considered in the next section. They are arranged in a folded configuration, and cross-couplings have been implemented in order to achieve two advanced frequency responses. It is worth noting that the design strategy that we have followed consists in, firstly, designing the filter (following the step-by-step procedure described in this section) without considering the cross-couplings of the component. Once all the mainline couplings have been designed, the different cross-couplings are added progressively, and the whole filter can then be built and optimized. It is also worth mentioning at this point that, when a cross-coupling is considered, only the dimensions related to the new added cross-coupling element should be optimized and, only if the target results are not recovered, the dimensions of nearby resonators are also considered for optimization.

F. IMPLEMENTATION OF THE AGGRESSIVE SPACE MAPPING TECHNIQUE

All the simulations described in the previous sections are performed employing the full-wave EM software tool FEST3D, by using a set of simulation parameters chosen to generate very fast simulations and low-precision results. In the filters designed in the next section, we have only considered 10 accessible modes to connect discontinuities, and 300 localized modes for their characterization (the meaning of these two computational parameters can be found in [34]). Therefore, the obtained low-accuracy frequency responses are not accurate enough for fabrication purposes. The well-known ASM technique presented in [31], however, enables us to recover the results in a precise but time-consuming space (fine model) using the results derived in the low-accuracy space (coarse model). In our two design examples, FEST3D is used as the coarse model, while the commercial

EM software Ansys HFSS is employed for recovering the results in the fine model. In most cases, only a few iterations are needed to recover the target frequency response of the filter in the fine space.

A summary of the main steps of the proposed design procedure can be found in Table 1.

III. DESIGN EXAMPLES

To illustrate the practical application of the procedure detailed in the previous section, we have considered next the design of two high-order generalized Chebyshev combine bandpass filters operating in the S-band. Both filters are arranged in a folded configuration, and cross-couplings have been implemented to achieve symmetric and asymmetric frequency responses including TZs located above and below the passband. In particular, the first design case is an 8-th order bandpass filter in a standard folded configuration, including 4 TZs (at real frequencies) located symmetrically below and above the filter passband (i.e., an 8-4-0 filter). The second example is an 8-th order bandpass filter arranged in a cul-de-sac configuration, exhibiting an asymmetric frequency response with 3 TZs at real frequencies and different rejection lobes, being one TZ located at the lower side of the passband, and the other two TZs located at the upper side (i.e., an 8-3-0 filter).

Since the passband of both filters is centred at $f_0 = 3$ GHz, the first step of the design procedure (see Section II-A) is common for both of them. The dimensions of the designed rectangular cavity are as follows (see Fig. 1): $a = 15$ mm, $b = 30$ mm and $l = 14$ mm. Besides, the height of the cylindrical post is of 22 mm, while its radius is equal to 2 mm. On the other hand, the calculated values for the equivalent lumped elements of the resonator are: $L = 13.236$ nH and $C = 0.213$ pF. In order to check the obtained values for the lumped elements, the reactance of the derived LC series resonant circuit is compared with the reactance of the real waveguide resonator. The results shown in Fig. 8 fully validate the followed approach.

A. FIRST DESIGN EXAMPLE: 8-4-0 FILTER

First, the design of an 8-th order generalized Chebyshev bandpass filter operating at $f_0 = 3$ GHz, with 22 dB of return losses and a bandwidth of 20 MHz, is addressed. In addition, to improve the filter selectivity, 4 TZs are introduced symmetrically in the frequency response by using cross-couplings between some resonators. The coupling and routing diagram of this filter is represented in Fig. 9, where all the couplings are of magnetic type, except for the coupling between resonators 3 and 6, which is of electric type. For the sake of clarity, the cross-couplings are drawn in Fig. 9 using dotted lines.

The TZs are included in the low-pass prototype at $s = \pm j1.2$ and at $s = \pm j1.7$, which produce 4 rejection lobes of 40 dB and 60 dB distributed on both the lower and the upper sides of the passband. The non-zero elements of the corresponding $N + 2$ coupling matrix

TABLE 1. Summary of the proposed design procedure.

Step	Description
(1)	Synthesis of the $N + 2$ coupling matrix according to the electrical specifications and filter configuration. Obtain a circuit model of the filter based on impedance inverters and L_0 - C_0 series networks (and FIRs, M_{ii} , for asymmetric designs).
(2)	Design of the isolated combine resonators at the frequencies given by the coupling matrix model according to equation (1) and Fig. 2. Calculation of their dimensions and derivation of an equivalent circuit in terms of an L - C series network (and a FIR only for asymmetric designs).
(3)	Scale the circuit model and obtain the new K -inverter values according to the L - C s obtained in the resonator designs and Z_0 of the input/output excitation using equations (2), (3) and (4).
(4)	Design of the coaxial excitation. Obtention of the relevant dimensions using the electrical response of the corresponding circuit model as a target (see Fig. 4).
(5)	Computation of the initial dimensions (width and height) of the coupling windows in order to match the K -inverter behaviour. For electric-type coupling windows, the response of the component shown in Fig. 5 is used for obtaining an initial value for the height (see [29] for more details on magnetic windows). To obtain the initial values for the windows widths, the inter-resonator coupling needs to be computed as a function of the window width. For filters with an asymmetric frequency response, the required coupling coefficient is obtained from the circuit model shown in Fig. 6, by choosing a very low value for the input/output inverter.
(6)	The filter resonators are added progressively one after the other. The dimensions of the physical structure considered in each stage are optimized by taking the group delay of the S_{11} parameter of the equivalent circuit model as the target response. The mainline couplings are designed first, and the cross-couplings are added progressively.
(7)	Implementation of the ASM technique to recover a set of filter dimensions which are accurate enough for fabrication purposes.

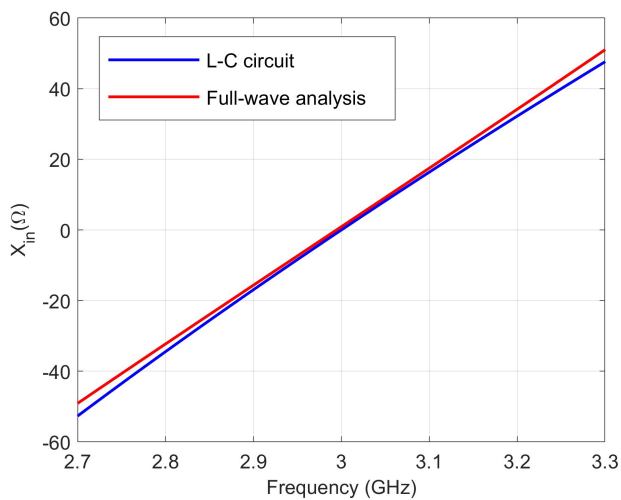


FIGURE 8. The reactance of the lumped elements equivalent circuit of the resonator is compared with the reactance of the real waveguide implementation.

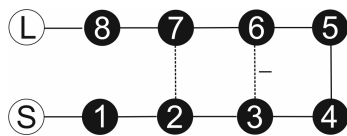


FIGURE 9. Coupling and routing diagram of the 8-4-0 bandpass filter.

for this design using a folded configuration (see Fig. 9) are: $M_{S1} = M_{8L} = 1.0231$, $M_{12} = M_{78} = 0.8440$, $M_{23} = M_{67} = 0.5919$, $M_{34} = M_{56} = 0.4834$, $M_{45} = 0.7842$, $M_{36} = -0.2894$, $M_{27} = 0.0320$. It is worth mentioning that, given a set of electrical specifications for a specific design, a particular coupling matrix is obtained. Therefore, if we want to add more transmission zeros to the electrical response, a different and appropriate coupling matrix should be synthesized, and additional cross-couplings should be considered in

the physical structure.

The circuit model of the filter can be derived starting from the obtained coupling matrix and the equivalent lumped elements of the resonators. Fig. 10 shows the equivalent circuit of the proposed filter, where Z_0 stands for the modal impedance of the coaxial line TEM mode (note that, since the filter is symmetric, FIRs are not included in the circuit model). The values of the LC lumped elements were obtained in the previous section, while the values (all in Ω) of the impedance inverters are: $K_{S1} = K_{8L} = 21.2788$, $K_{12} = K_{78} = 1.4043$, $K_{23} = K_{67} = 0.985$, $K_{34} = K_{56} = 0.8094$, $K_{45} = 1.2964$, $K_{36} = -0.4707$, and $K_{27} = 0.0517$ (note that the required coupling coefficients k_{ij} can be calculated, as stated in Section II-D, in terms of K_{ij} and the resonator slope parameter $\chi = Lw_0$). The electrical response (S -parameters) of this ideal circuit is displayed in Fig. 11. Furthermore, the physical realization of this filter in combine technology is shown in Fig. 12, where it is worth noting that the electric coupling between resonators 3 and 6 (see also Fig. 9) has been implemented using a rectangular window placed at the open end of the resonator [4].

According to the design procedure described in Section II, the next step consists in designing the coaxial excitation. The input/output resonators will be fed using 50Ω commercial coaxial connectors (inner and outer radii equal to 0.82 mm and 2.625 mm, respectively, and $\epsilon_r = 2.1$). In this stage, only the first resonator of the filter fed by the coaxial line is considered (see Fig. 4, left). Next, the group delay of the S_{11} parameter of the circuit model of this component (see Fig. 4, right) is considered as the target response. Only 3 parameters are optimized in this stage: d , h_1 and l_p (see Fig. 12 for the definition of these dimensions). After the optimization, the results shown in Fig. 13 are obtained, where a very good agreement can be observed between the full-wave and target responses. The following optimized dimensions (all in mm) are obtained at the end of this stage: $d = 10$, $h_1 = 22$ and $l_p = 4.28$.

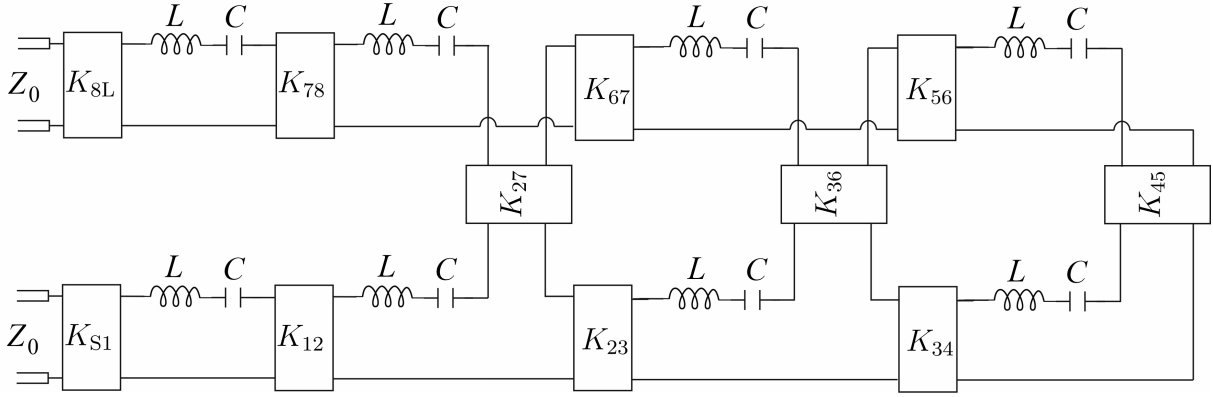


FIGURE 10. Equivalent circuit model of the 8-4-0 filter in terms of LC series resonators and ideal impedance inverters.

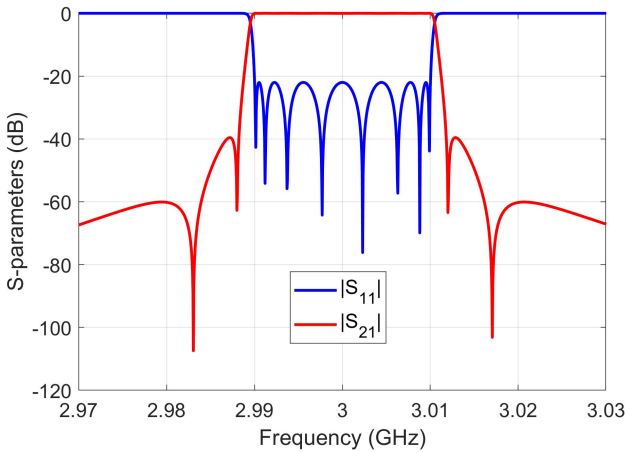


FIGURE 11. S-parameters of the equivalent circuit displayed in Fig. 10.

Afterwards, a set of initial values for the coupling windows is derived following the procedure explained in Section II-D. The obtained height of the magnetic-type coupling windows is $h_{wm} = 9.3$ mm, while the height of the electric coupling window has been set to $h_{we} = 14$ mm in order to achieve the required electric coupling (in this particular case, h_{we} and h_{wm} will not be optimized in the following steps). Furthermore, if w_{mn} refers to the width of the coupling window between the m -th and n -th resonators (see Fig. 12), the obtained initial values (all in mm) are: $w_{12} = w_{78} = 5.5$, $w_{23} = w_{67} = 4.85$, $w_{34} = w_{56} = 4.45$, $w_{45} = 5.9$, $w_{27} = 2.1$ and $w_{36} = 6.2$.

Next, since the filter is symmetric, we will firstly design the connection of the first 4 resonators (i.e., the lower branch of the routing diagram in Fig. 9) without considering the cross-couplings of the filter. These resonators will be added progressively, one after another, following the guidelines described in Section II-E, and using the results of previous stages as initial values of the next one. In each stage, the electrical response of the corresponding waveguide structure is optimized considering the response of the related circuit

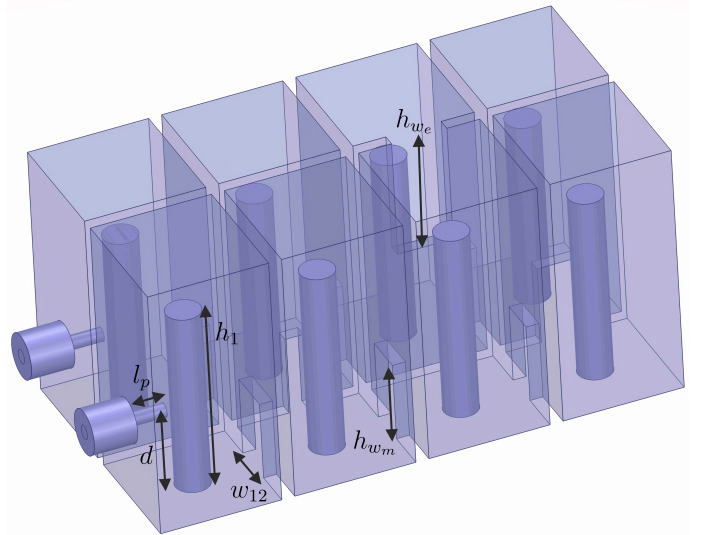


FIGURE 12. Physical realization in combline technology of the 8-4-0 bandpass filter whose coupling diagram is shown in Fig. 9.

model (which can be easily derived from the circuit in Fig. 10) as a target. Fig. 14 shows the results of the optimization process after adding the first 4 resonators (connection S-1-2-3-4), where a very good agreement between the full-wave response and the target curve can be observed (the results concerning the connection of the first 2 and 3 resonators have been omitted for the sake of brevity). In addition, the dimensions of the waveguide component are also reported in Table 2 (h_i stands for the height of the i -th resonator post).

TABLE 2. Optimized dimensions (in mm) of the waveguide component obtained after connecting the first 4 resonators of the 8-4-0 filter.

Parameter	h_1	h_2	h_3	h_4	w_{12}
Value	21.830	22.226	22.271	22.385	5.416
Parameter	w_{23}	w_{34}	l_p	d	
Value	4.766	4.463	4.216	9.995	

In the next step of the design process, we can address the

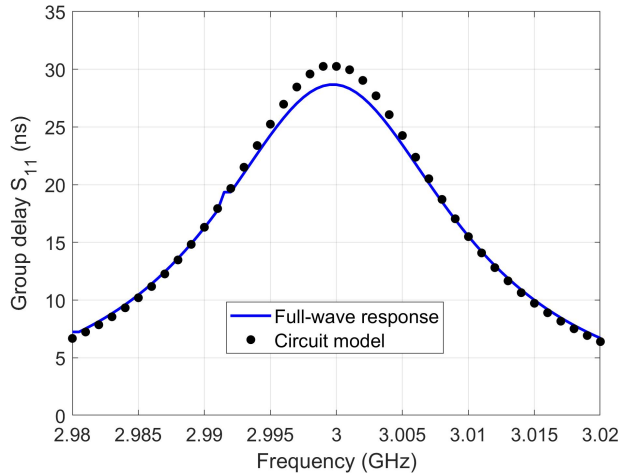


FIGURE 13. Results of the optimization after designing the coaxial excitation of the 8-4-0 filter.

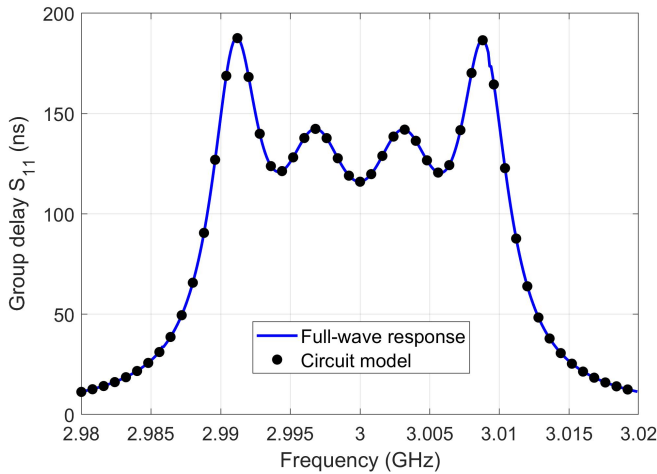


FIGURE 14. Results of the optimization considering the first 4 resonators (S-1-2-3-4) of the 8-4-0 filter.

optimization of the whole filter since the component is symmetric. However, cross-couplings will not be included yet and only the mainline couplings will be taken into account. Therefore, the direct connection of the 8 resonators of the filter following the routing diagram shown in Fig. 9 (without the cross-couplings K_{27} and K_{36}) is considered next. The initial dimensions of the structure have been reported in Table 2. This time, the electrical response to be optimized is based on the magnitude of the S_{11} and S_{21} parameters. The results of the optimization are displayed in Fig. 15, where the response of the equivalent circuit model is successfully compared with the response of the waveguide component. Moreover, the new optimized dimensions of the structure are reported in Table 3 (note that, since the filter is symmetric, only the relevant dimensions are shown in the table).

In the next step, the electric coupling between resonators 3 and 6 is added (see also Fig. 9). The S -parameters of the

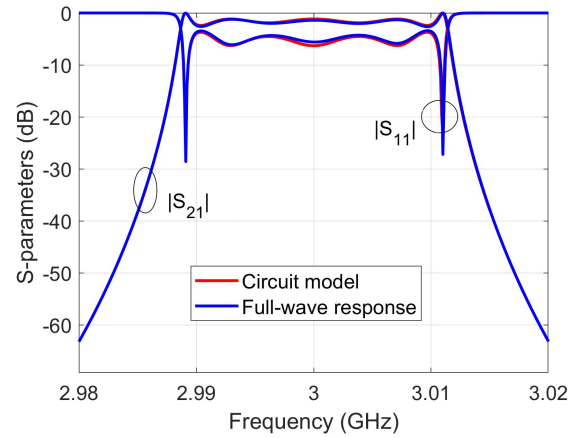


FIGURE 15. Results of the optimization considering the connection (without cross-couplings) of the 8 resonators of the 8-4-0 filter.

TABLE 3. Optimized dimensions (in mm) of the waveguide component obtained after connecting (without cross-couplings) the 8 resonators of the 8-4-0 filter.

Parameter	h_1	h_2	h_3	h_4	w_{12}
Value	21.828	22.242	22.284	22.373	5.378
Parameter	w_{23}	w_{34}	w_{45}	l_p	d
Value	4.754	4.381	5.856	4.223	10.041

optimized waveguide component compared with the electrical response of the corresponding circuit model are shown in Fig. 16, where a very good agreement can be again observed. Finally, the magnetic coupling between resonators 2 and 7

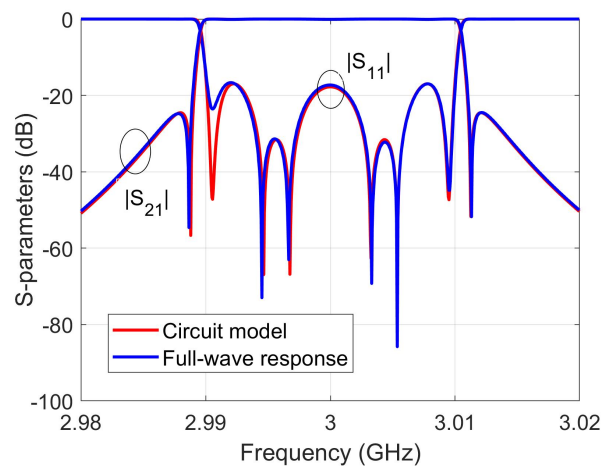


FIGURE 16. Results of the optimization considering all the couplings of the 8-4-0 filter except for the magnetic cross-coupling 2-7.

is added to the structure, and the optimization of the whole bandpass filter can be addressed. The electrical response of the designed filter is shown in Fig. 17, where a very good agreement can be observed between the responses of the circuit model and waveguide component. The dimensions of

the designed filter are summarized in Table 4 (note that the filter is symmetric).

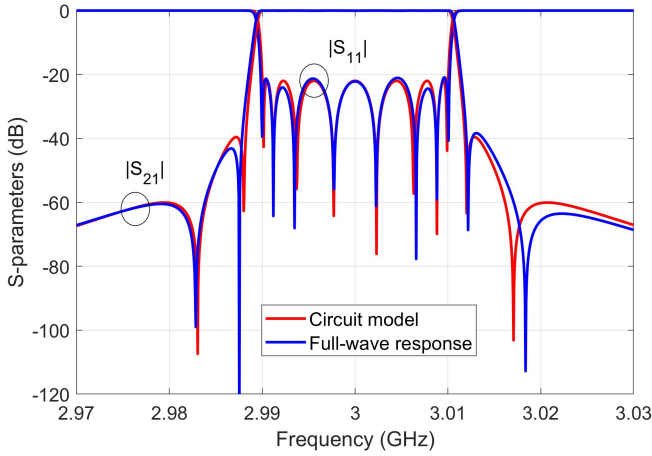


FIGURE 17. Electrical response of the designed 8-4-0 bandpass filter (low-precision design).

TABLE 4. Dimensions (in mm) of the 8-4-0 bandpass filter (low-precision design).

Parameter	h_1	h_2	h_3	h_4
Value	21.821	22.218	22.340	22.271
Parameter	w_{12}	w_{23}	w_{34}	w_{45}
Value	5.443	4.775	4.444	5.813
Parameter	w_{27}	w_{36}	l_p	d
Value	2.109	6.427	4.226	10.024

As we explained in Section II-F, the filter dimensions reported in Table 4 provide us with a low-precision design. However, a high-precision design can be recovered by using the ASM technique (the commercial EM software Ansys HFSS is used for the simulations performed in the fine space). The final results obtained in the high-precision space (Ansys HFSS) are shown in Fig. 18, where 8 iterations of the ASM technique have been needed to recover the previous results obtained in the coarse or low-precision space (FEST3D results). A very good agreement can be observed, thus confirming the accuracy of the ASM results. Table 5 collects the final dimensions of the designed filter. These values are very close to the dimensions obtained in the coarse space (see also Table 4).

TABLE 5. Dimensions (in mm) of the 8-4-0 bandpass filter (high-precision design).

Parameter	h_1	h_2	h_3	h_4
Value	21.846	22.215	22.335	22.267
Parameter	w_{12}	w_{23}	w_{34}	w_{45}
Value	5.439	4.754	4.435	5.838
Parameter	w_{27}	w_{36}	l_p	d
Value	2.138	6.402	4.203	10.003

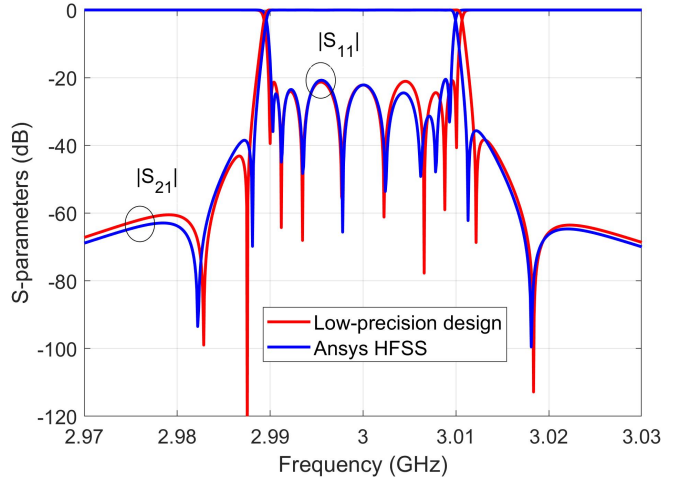


FIGURE 18. Electrical response of the designed 8-4-0 bandpass filter (high-precision design).

B. SECOND DESIGN EXAMPLE: 8-3-0 CUL-DE-SAC BANDPASS FILTER

Next, we address the design of an 8-th order generalized Chebyshev bandpass filter arranged in a cul-de-sac configuration exhibiting an asymmetric response. The passband is centred at $f_0 = 3$ GHz, with 23 dB of return losses and a bandwidth of 16.7 MHz. In this case, 3 TZs are introduced in the frequency response, one at the lower side of the passband ($s = -j1.326$ in the low-pass prototype, producing a rejection lobe of 40 dB), and a pair at the upper side ($s = j1.29$ and $s = j1.472$ in the low-pass prototype, generating two rejection lobes of 60 dB). The coupling and routing diagram of this filter is represented in Fig. 19, where all the couplings are of magnetic type, except for the coupling between resonators 2 and 6, which is of electric type (the cross-couplings have been depicted in Fig. 19 using dotted lines).

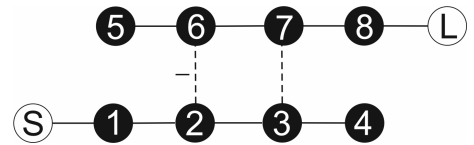


FIGURE 19. Coupling and routing diagram of the 8-3-0 cul-de-sac bandpass filter.

The non-zero elements of the $N + 2$ coupling matrix for this design using a cul-de-sac configuration are: $M_{11} = M_{88} = 0.0054$, $M_{22} = M_{77} = 0.0059$, $M_{33} = -0.1376$, $M_{44} = 0.4551$, $M_{55} = -0.8707$, $M_{66} = 0.1190$, $M_{S1} = M_{8L} = 1.044$, $M_{12} = M_{78} = 0.8644$, $M_{23} = 0.3970$, $M_{34} = 0.7054$, $M_{56} = 0.3485$, $M_{67} = 0.4510$, $M_{26} = -0.4510$, $M_{37} = 0.3970$. On the other hand, the equivalent circuit model of the filter is shown in Fig. 20, where the values (all in Ω) of the impedance inverters are: $K_{S1} = K_{8L} = 19.8176$, $K_{12} = K_{78} = 1.1981$, $K_{23} =$

0.5503, $K_{34} = 0.9777$, $K_{56} = 0.483$, $K_{67} = 0.6252$, $K_{26} = -0.6252$, and $K_{37} = 0.5503$. In this case, since the diagonal elements of the coupling matrix (M_{ii}) are not equal to zero, the equivalent circuit of Fig. 20 must include FIRs in the corresponding resonators. According to (4), the next values (all in Ω) for these FIRs are obtained: $X_1 = X_8 = 0.0075$, $X_2 = X_7 = 0.0081$, $X_3 = -0.1908$, $X_4 = 0.6308$, $X_5 = -1.2069$, and $X_6 = 0.1649$. Then, following the numerical procedure given at the end of Section II-D, the next values for all the filter coupling coefficients are obtained: $k_{12} = 0.0048$, $k_{23} = 0.0022$, $k_{34} = 0.0039$, $k_{56} = 0.0019$, $k_{67} = 0.0024$, $k_{78} = 0.0048$, $k_{26} = -0.0025$ and $k_{37} = 0.0022$. The S -parameters of this ideal circuit are shown in Fig. 21, while its physical realization can be found in Fig. 1.

Next, the design of the coaxial excitation of the filter is addressed (input/output resonators are fed using the same coaxial line that we employed in the previous design). In this stage, only the first resonator of the filter (fed by the coaxial line) is considered, and the height h_1 of the post, as well as the dimensions d_1 and l_{p1} (see Fig. 1) are optimized based on the response of its equivalent circuit (see Fig. 4). The following optimized dimensions (all in mm) are obtained at the end of this stage: $d_1 = 9.917$, $h_1 = 22.076$ and $l_{p1} = 4.148$. It is worth noting that, although this filter is not symmetric, the design of the coaxial excitation for the input and output resonators provides the same initial values, since $K_{S1} = K_{8L}$. However, the dimensions of the input/output resonators related to the coaxial excitation will be optimized independently afterwards.

In the next stage of the design process, a set of initial values for the coupling windows is determined. As explained in Section II-D, the 2-port asymmetric structures considered in this stage must include resonators with different values for their post heights. The obtained initial values (in mm) for the cited heights, which have been evaluated taking into account the resonant frequencies of the circuit model resonators, are: $h_1 = h_2 = h_7 = h_8 = 22.076$, $h_3 = 22.084$, $h_4 = 22.048$, $h_5 = 22.129$, $h_6 = 22.069$. By following the design procedure explained in Section II-D, an initial value of $h_{w_m} = 9.3$ mm is obtained for the height of all magnetic windows (this dimension will not be optimized in the following steps). For the electric-type coupling window, we obtain $h_{w_e} = 10$ mm. Furthermore, the obtained initial values (in mm) for the widths of the coupling windows are: $w_{12} = w_{78} = 5.15$, $w_{23} = 4$, $w_{34} = 4.8$, $w_{56} = 3.78$, $w_{67} = 4.1$, $w_{26} = 7$, and $w_{37} = 4.15$.

As the filter is not symmetric, the design strategy consists in splitting the design process in three main steps. Firstly, the connection of resonators S-1-2-3-4 will be addressed (i.e., the lower branch of the coupling diagram in Fig. 19). Next, the connection of resonators 5-6-7-8-L will be considered (i.e., the upper branch of the coupling diagram in Fig. 19). Finally, the cross-couplings between resonators 2-6 and 3-7 will be added one after another. In each of these three main steps, the resonators will be added progressively, and the dimensions of the corresponding waveguide components will be optimized

considering the electrical response of the equivalent circuit model as the target response.

Fig. 22 shows the results of the optimization after connecting the resonators S-1-2-3-4, compared with the response of the corresponding ideal circuit. The dimensions of the physical structure can be found in Table 6, where h_i is the height of the i -th resonator post, and w_{mn} stands for the width of the coupling windows connecting the m -th and n -th resonators (see also Fig. 1).

TABLE 6. Dimensions (in mm) of the structure after optimizing the connection of resonators S-1-2-3-4.

Parameter	h_1	h_2	h_3	h_4	w_{12}
Value	21.894	22.276	22.288	22.366	5.179
Parameter	w_{23}	w_{34}	l_{p1}	d_1	
Value	3.892	4.825	4.073	10.218	

On the other hand, Fig. 23 shows the results of the design of the waveguide component representing the connection of resonators 5-6-7-8-L. Once again, a very good agreement is obtained between the full-wave response of the structure and the response of the equivalent circuit model. The optimized dimensions of the component are reported in Table 7.

TABLE 7. Dimensions (in mm) of the structure after optimizing the connection of resonators 5-6-7-8-L.

Parameter	h_5	h_6	h_7	h_8	w_{56}
Value	22.412	22.334	22.267	21.877	3.805
Parameter	w_{67}	w_{78}	l_{p2}	d_2	
Value	4.136	5.172	4.116	10.213	

After designing the second half of the filter, the magnetic coupling between resonators 3 and 7 is considered (see also Fig. 19). Fig. 24 shows the optimized results of the S -parameters (compared with the electrical response of the corresponding circuit model) after adding this coupling window. An excellent agreement between both responses is again observed.

In the last step of the design process, the electric coupling between resonators 2 and 6 is added to the structure, so the design of the whole filter can be addressed. As we stated before, the required electric coupling between resonators 2 and 6 results in a coupling window whose initial values for the height and width are $h_{w_e} = 10$ mm and $w_{26} = 7$ mm, respectively. With these initial values, however, it was not possible to recover the ideal response of the whole filter. In fact, the results we achieved using such initial values are shown in Fig. 25 with red lines. With the aim of obtaining a better initial point, a new re-optimization of the window dimensions was performed, thus finding the following new values: $h_{w_e} = 12$ mm and $w_{26} = 11$ mm. As we can check from Fig. 25 (see the new results with black lines), a very good starting point was finally obtained. This change in the dimensions of the electric-type coupling window was due to the stronger effect of the adjacent resonators in such coupling topology.

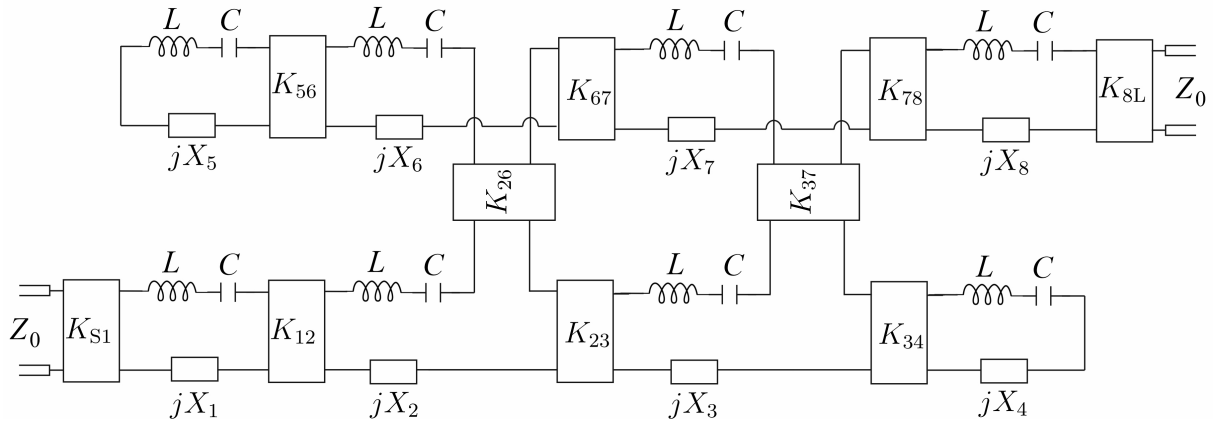


FIGURE 20. Equivalent circuit model of the cul-de-sac bandpass filter in terms of ideal impedance inverters, LC series resonators and FIRs.

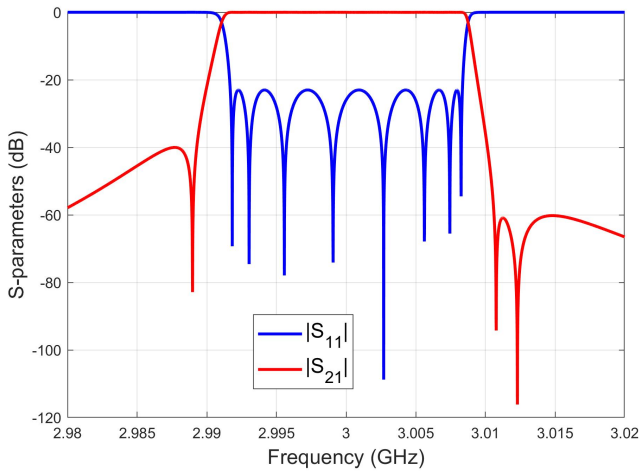


FIGURE 21. Electrical response of the circuit model of the cul-de-sac bandpass filter.

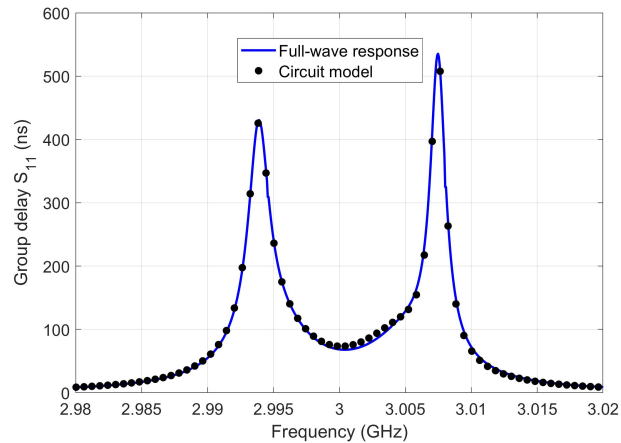


FIGURE 22. Results of the optimization after designing the connection S-1-2-3-4 of the 8-3-0 filter.

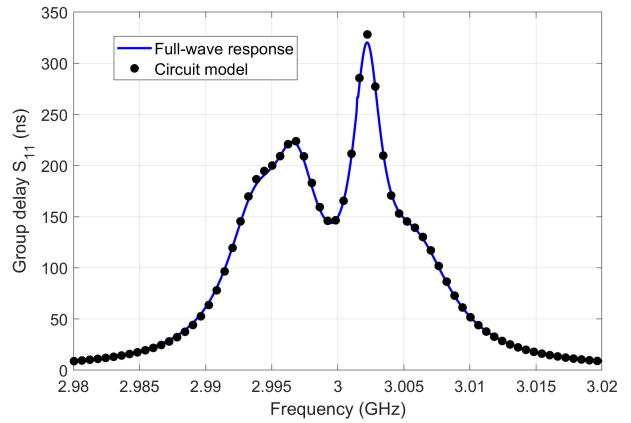


FIGURE 23. Results of the optimization after designing the connection 5-6-7-8-L of the 8-3-0 filter.

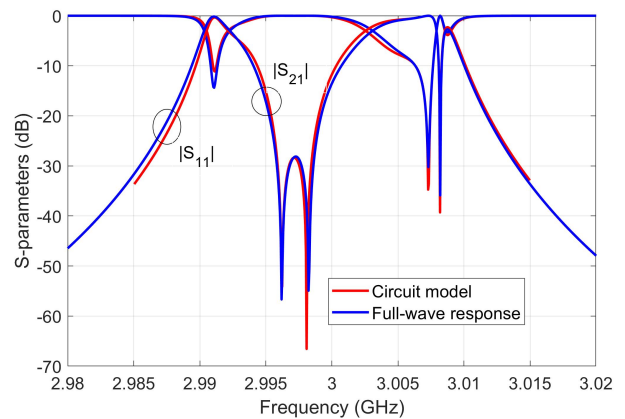


FIGURE 24. Results of the optimization after adding the magnetic coupling 3-7 to the 8-3-0 filter.

The results of the optimization of the S -parameters of the complete filter (low-precision design) are successfully compared with the ideal circuit response in Fig. 26, while

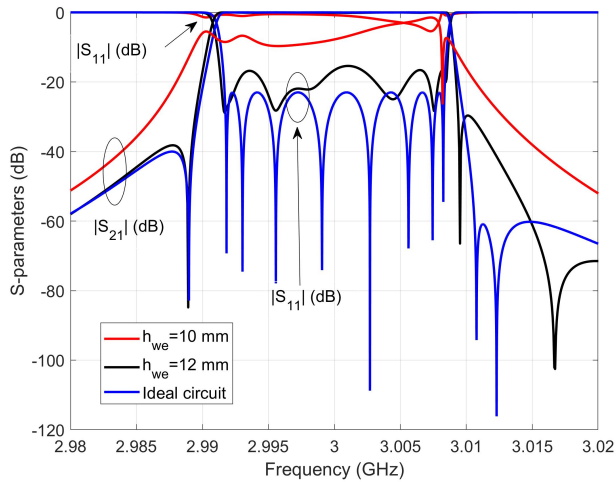


FIGURE 25. Performance of the S -parameters of the 8-3-0 filter for different dimensions of the electric window connecting resonators 2 and 6.

the dimensions of the final design are reported in Table 8.

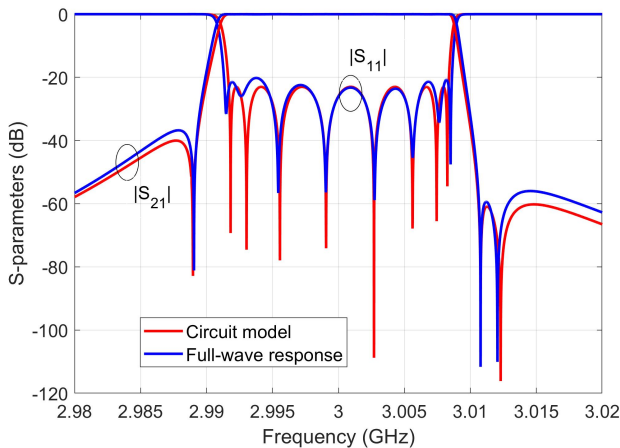


FIGURE 26. Electrical response of the designed 8-3-0 cul-de-sac bandpass filter (low-precision design).

TABLE 8. Dimensions (in mm) of the 8-3-0 cul-de-sac bandpass filter (low-precision design).

Parameter	h_1	h_2	h_3	h_4	h_5
Value	21.876	22.356	22.224	22.428	22.365
Parameter	h_6	h_7	h_8	w_{12}	w_{23}
Value	22.419	22.214	21.896	5.191	3.918
Parameter	w_{34}	w_{56}	w_{67}	w_{78}	w_{26}/h_{we}
Value	4.785	3.764	4.102	5.116	10.740/12.180
Parameter	w_{37}	l_{p1}	l_{p2}	d_1	d_2
Value	4.286	4.108	4.075	10.267	10.262

The last stage of the design process consists in applying the ASM technique, in order to get a set of dimensions that provide us with a high-precision design. A very good matching with the response of the low-precision design has

been obtained after 11 iterations of the ASM technique, as shown in Fig. 27, where the results obtained in the high-precision space (Ansys HFSS) are displayed and compared with the response of the low-precision design. The dimensions obtained in the high-precision space, which are reported in Table 9, are very close to the ones derived in the coarse space (see also Table 8).

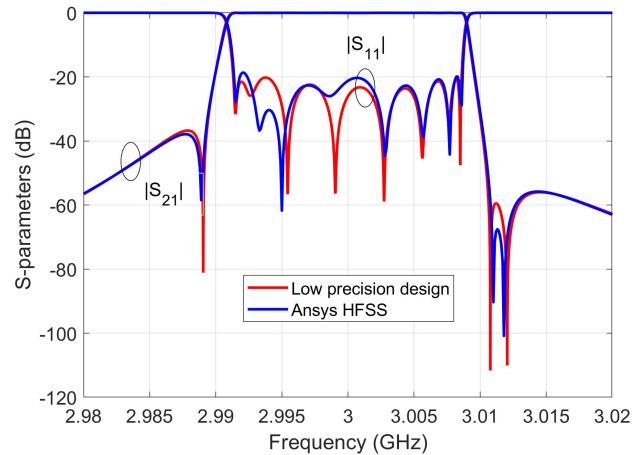


FIGURE 27. Electrical response of the designed 8-3-0 cul-de-sac bandpass filter (high-precision design).

TABLE 9. Dimensions (in mm) of the 8-3-0 cul-de-sac bandpass filter (high-precision design).

Parameter	h_1	h_2	h_3	h_4	h_5
Value	21.890	22.346	22.213	22.408	22.354
Parameter	h_6	h_7	h_8	w_{12}	w_{23}
Value	22.410	22.204	21.925	5.228	3.970
Parameter	w_{34}	w_{56}	w_{67}	w_{78}	w_{26}/h_{we}
Value	4.855	3.821	4.142	5.172	10.793/12.231
Parameter	w_{37}	l_{p1}	l_{p2}	d_1	d_2
Value	4.339	4.107	4.044	10.248	10.238

As a final validation check of the complete design procedure, the cul-de-sac filter designed in the high-precision space has also been analyzed with a second full-wave EM commercial simulator (CST Studio Suite). The obtained results, which can be seen in Fig. 28, show a good agreement between CST and HFSS responses. The minor differences between both simulators results are reasonable, since a filter response with a very narrow passband (0.56% of fractional bandwidth) has been obtained using two EM software tools based on different numerical analysis methods.

Finally, we have compared the electrical performance and complexity of the two designed filters with other similar combline and coaxial filters found in the technical literature, in terms of several parameters: order N of the designed filter, topology of the filter (inline, folded arrangement, etc.), presence of transmission zeros, and symmetry or asymmetry of the filter response. We have also included in this comparison the technique used in the design procedure (classical, as explained in Section I, or based on a segmentation of the

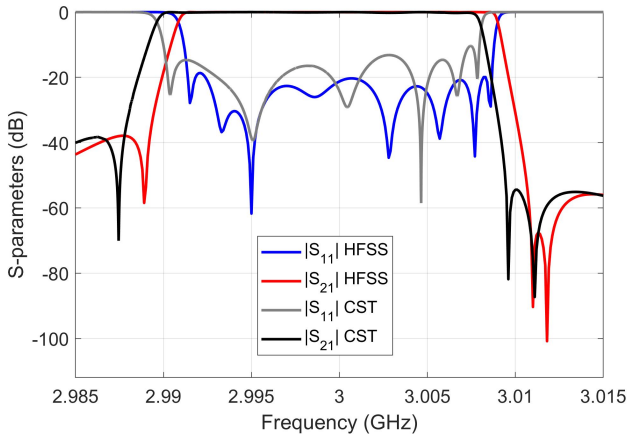


FIGURE 28. Ansys HFSS and CST Studio Suite electrical responses of the designed 8-3-0 filter.

structure), as well as the technology employed for implementing the filter. The summary of this comparison can be found in Table 10, where it can be seen that higher order and very selective responses, as well as complex topologies (such as the cul-de-sac one), have been successfully considered in this work.

IV. EXPERIMENTAL VALIDATION

As an experimental validation of the proposed design procedure, the 8-4-0 filter example considered in Section III-A has been manufactured in aluminum. However, before implementing the filter prototype, some important practical issues must be taken into account.

First, since we will resort to a low-cost fabrication technique (i.e., standard milling), rounded corners (radius of 2.5 mm) must be considered in all the cavities of the filter to account for undesired mechanization effects. Besides, tuning screws will be needed both in cavities (diameter of 4 mm) and coupling windows (diameter of 2 mm, except for the screw used in the 2-7 coupling window, whose diameter is found to be of 1.6 mm). Furthermore, the size of the flange of the coaxial connector that we have used (Radiall® TNC-18 connector) is equal to 19 mm, so a minimum gap of 19 mm is needed between adjacent connectors. However, the available space between the center of the input/output ports in our design (see Fig. 12) is of 16.5 mm. As a consequence, the coaxial connectors need to be shifted to the side faces of the structure. Since all these issues must be considered before manufacturing the prototype, the filter needs, first, to be slightly fixed. Fig. 29 shows the new design of the 8-4-0 filter, including rounded corners, tuning screws and input/output ports located on the sides of the component.

The new dimensions (in mm) of the modified 8-4-0 filter (high-precision design), considering all prior practical aspects, are collected in Table 11, where the notation for the different variables is the same of Section III.

A photograph of the manufactured filter can be found in

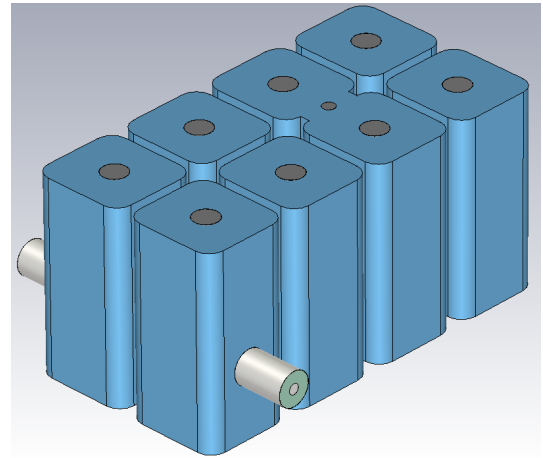


FIGURE 29. Modified 8-4-0 filter with rounded corners, tuning screws and input/output ports located on the side faces of the component.

Fig. 30, while Fig. 31 shows a comparison between the simulated response (without considering metal losses) and the measured data. An acceptable agreement has been obtained, and a very good performance in terms of the measured return losses can be observed. Although the transmission zeros are not clearly marked in the measured response, their presence (and location) can be easily inferred from the experimental results.

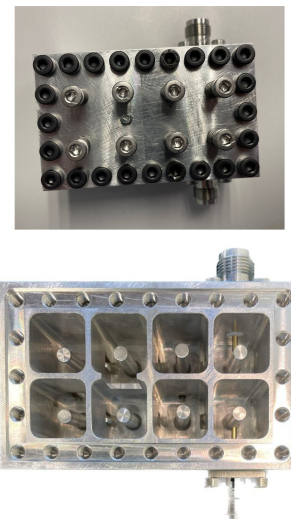


FIGURE 30. Photograph of the manufactured 8-4-0 filter: assembled component (top) and body without cover (bottom).

It is worth noting that, based on our previous experience with the prototype manufacturer, we are aware that the real conductivity of the material (aluminum) used in the fabricated filter is lower than the well-known nominal value, thus obtaining an in-band performance with higher insertion losses than expected (also due to the narrowband nature of the designed filter). Therefore, we have proceeded to simulate

TABLE 10. Comparison of the two designed comblines filters with similar designs found in the technical literature.

Ref.	Order (N)	Topology	TZs	Symmetry	Design procedure	Technology
[4]	4	Folded	2	Symm.	Classical	Comblines
[6]	5	Inline	2	Asymm.	Classical	Comblines (cylindrical cavity)
[7]	5	Inline	No	Symm.	Classical	Comblines
[8]	4	Inline	No	Symm.	Classical	Comblines
[9]	10	Inline	No	Symm.	Classical	Comblines
[10]	4	Inline	No	Symm.	Classical	Comblines (dielectric tuning rod)
[11]	4	Inline	No	Symm.	Classical	Comblines (dielectric tuners)
[12]	4	Folded	2	Symm.	Segmentation (input impedance phase)	Comblines
[14]	3 and 4	Inline and folded	2	Symm.	Classical	Coaxial inset resonator
[16]	5	Inline	2	Symm.	Classical	Comblines
[17]	3	Triangle shape	3	Asymm.	Classical	Comblines
This work	8	Folded	4	Symm.	Segmentation (reflected group delay)	Comblines
This work	8	Cul-de-sac	3	Asymm.	Segmentation (reflected group delay)	Comblines

TABLE 11. Dimensions (in mm) of the modified 8-4-0 bandpass filter.

Parameter	h_1	h_2	h_3	h_4
Value	21.693	22.067	22.161	22.096
Parameter	w_{12}	w_{23}	w_{34}	w_{45}
Value	5.107	4.431	4.104	5.523
Parameter	w_{27}	w_{36}	l_p	d
Value	2.100	8.902	4.537	10.834

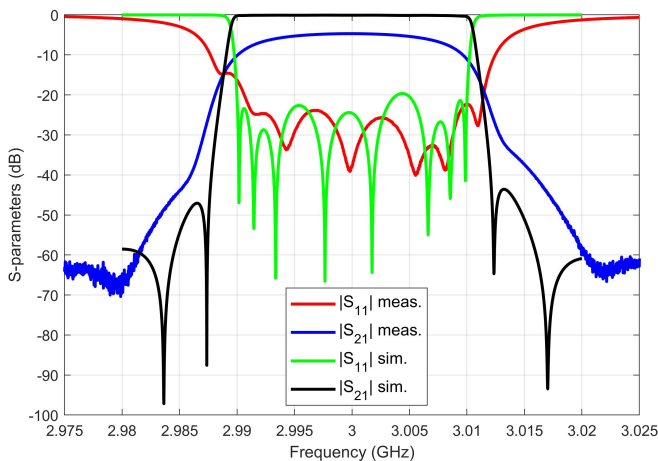


FIGURE 31. Simulated response (no losses) compared to the measured data.

the designed filter considering the metal losses, by using in the simulation tool a material whose conductivity value ($\sigma = 8.67 \cdot 10^6$ S/m) provides the same level of insertion losses as in the measured response. The obtained results are shown in Fig. 32, where a very good agreement is now observed between both sets of data. It is also worth mentioning that, as we already observed with the measured data, transmission zeros are not either clearly visible in the simulated response when losses are considered in the full-wave analysis tool.

V. CONCLUSION

In this paper, an efficient procedure to design high-order comblines bandpass filters with advanced electrical responses, and including transmission zeros, has been presented. The

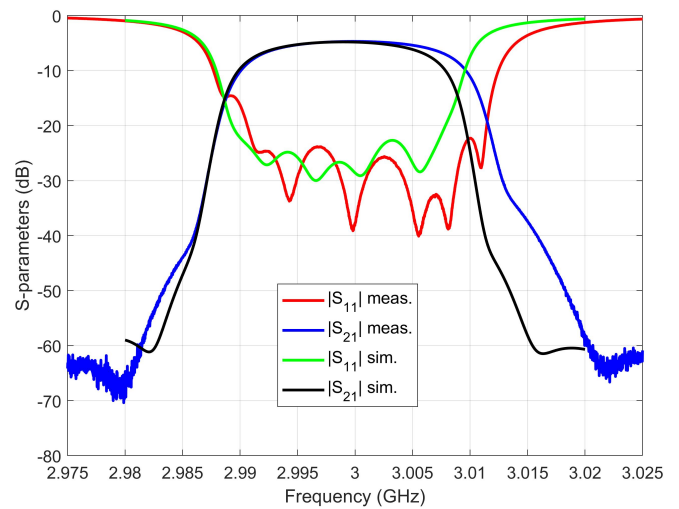


FIGURE 32. Simulated response considering metal losses ($\sigma = 8.67 \cdot 10^6$ S/m) compared to the measured data.

design process, which is based on a proper segmentation strategy of the complete filter structure, relies on the use of equivalent circuit models that provide the target electrical responses needed in each stage of the proposed method. Moreover, the ASM technique has allowed to implement the design procedure with a low-accuracy EM solver, thus finally obtaining a very accurate solution for the designed filters with a reduced number of high-accuracy simulations. In order to validate the proposed design procedure, two complex comblines bandpass filters, one of them in a cul-de-sac configuration exhibiting an asymmetric frequency response, have been successfully designed using full-wave commercial simulation tools. Furthermore, as an experimental verification, a prototype of the 8-4-0 bandpass filter has been manufactured, obtaining a good agreement between the simulated and measured responses, thus fully validating the proposed design procedure.

REFERENCES

- [1] P. Pramanick and P. Bhartia, *Modern RF and Microwave Filter Design*. Norwood, MA, USA: Artech House, 2016.
- [2] R. J. Cameron, C. M. Kudsia, and R. R. Mansour, *Microwave Filters for Communication Systems: Fundamentals, Design, and Applications*, 2nd ed. Hoboken, NJ, USA: Wiley, 2018.
- [3] P. Vallerotonda, L. Pelliccia, C. Tomassoni, F. Cacciamani, R. Sorrentino, J. Galdeano, and C. Ernst, "Compact waveguide bandpass filters for broadband space applications in C and Ku-bands," in *2019 Eur. Microw. Conf. Central Europe (EuMCE)*, May 2019, pp. 116–119.
- [4] M. El Sabbagh, K.A. Zaki, H.-W. Yao, and M. Yu, "Full-wave analysis of coupling between combine resonators and its application to combine filters with canonical configurations," *IEEE Trans. Microw. Theory Techn.*, vol. 49, no. 12, pp. 2384–2393, Dec. 2001.
- [5] S. Sirci, E. Menargues, and S. Berry, "Triangular combine filters conceived for additive manufacturing," in *2021 IEEE MTT-S Int. Microw. Filter Workshop (IMFW)*, Nov. 2021, pp. 151–154.
- [6] R. Tkadlec and G. Macchiarella, "Pseudoelliptic combine filter in a circularly shaped tube," in *2018 IEEE MTT-S Int. Microw. Symp. (IMS)*, 2018, pp. 1099–1102.
- [7] C. Kwak, M. Uhm, and I. Yom, "Feasibility study on combine filter for tunable filters," in *2013 Asia-Pacific Microw. Conf. Proc. (APMC)*, 2013, pp. 927–929.
- [8] S. Nassar, P. Meyer, and P. W. van der Walt, "An S-band combine filter with reduced size and increased pass-band separation," in *2015 Conf. Microw. Techn.*, 2015, pp. 1–4.
- [9] Z. Qi, J. Zeng, and X. Li, "A compact combine filter design and optimization using the Cauchy method," in *2016 IEEE Int. Conf. Microw. Millimeter Wave Technol. (ICMMT)*, vol. 1, 2016, pp. 232–234.
- [10] G. B. and R. R. Mansour, "A tunable quarter-wavelength coaxial filter with constant absolute bandwidth using a single tuning element," *IEEE Microw. Wirel. Compon. Lett.*, vol. 31, no. 6, pp. 658–661, 2021.
- [11] A. Sharma, S. Cogollos, V. E. Boria, and M. Guglielmi, "Analysis and design of re-configurable combine filters using dielectric tuners," in *2021 51st Eur. Microw. Conf. (EuMC)*, 2022, pp. 122–125.
- [12] H. Jia and R. R. Mansour, "An efficient technique for tuning and design of filters and diplexers," *IEEE Trans. Microw. Theory Techn.*, vol. 68, no. 7, pp. 2610–2624, July 2020.
- [13] A. Widaa, C. Bartlett, and M. Höft, "Design of compact quasi-elliptic bandpass filters based on coaxial inset resonators," *IEEE Access*, vol. 11, pp. 18 739–18 749, 2023.
- [14] —, "Tunable coaxial bandpass filters based on inset resonators," *IEEE Trans. Microw. Theory Techn.*, vol. 71, no. 1, pp. 285–295, 2023.
- [15] J. J. Vague, D. Rubio, M. A. Fuentes, S. Cogollos, M. Baquero, V. E. Boria, and M. Guglielmi, "Inline combine filters of order N with up to N+1 transmission zeros," *IEEE Trans. Microw. Theory Techn.*, vol. 69, no. 7, pp. 3287–3297, July 2021.
- [16] M. Yuceer, "A reconfigurable microwave combine filter," *IEEE Trans. Circuits Syst. II: Express Briefs*, vol. 63, no. 1, pp. 84–88, 2016.
- [17] J.-X. Xu, L. Yang, Y. Yang, and X. Y. Zhang, "High-Q-factor tunable bandpass filter with constant absolute bandwidth and wide tuning range based on coaxial resonators," *IEEE Trans. Microw. Theory Techn.*, vol. 67, no. 10, pp. 4186–4195, 2019.
- [18] P. Zhao and M. Rao, "Design and tuning of extracted-pole filters with non-resonant nodes by circuit model extraction," *IEEE Trans. Microw. Theory Techn.*, vol. 70, no. 4, pp. 2174–2184, Apr. 2022.
- [19] R. J. Cameron, A. Harish, and C. J. Radcliffe, "Synthesis of advanced microwave filters without diagonal cross-couplings," *IEEE Trans. Microw. Theory Techn.*, vol. 50, no. 12, pp. 2862–2872, Dec. 2002.
- [20] R. J. Cameron, "General coupling matrix synthesis methods for Chebyshev filtering functions," *IEEE Trans. Microw. Theory Techn.*, vol. 47, no. 4, pp. 433–442, Apr. 1999.
- [21] R. J. Cameron, Y. Wang, and M. Yu, "Direct-coupled realizations for microwave bandstop filters," in *IEEE MTT-S Int. Microw. Symp. Dig.*, June 2005, pp. 111–114.
- [22] W. M. Fathelbab, "Synthesis of cul-de-sac filter networks utilizing hybrid couplers," *IEEE Microw. Wirel. Compon. Lett.*, vol. 17, no. 5, pp. 334–336, May 2007.
- [23] D. G. Swanson, "Some observations on the coupling matrix," in *2021 IEEE MTT-S Int. Microw. Filter Workshop*, 2021, pp. 172–174.
- [24] H.-W. Yao, K.A. Zaki, A. E. Atia, and R. Hershtig, "Full wave modeling of conducting posts in rectangular waveguides and its applications to slot coupled combine filters," *IEEE Trans. Microw. Theory Techn.*, vol. 43, no. 12, pp. 2824–2830, Dec. 1995.
- [25] J. Ness, "A unified approach to the design, measurement, and tuning of coupled-resonator filters," *IEEE Trans. Microw. Theory Techn.*, vol. 46, no. 4, p. 343–351, 1998.
- [26] P. D. Laforge, R. R. Mansour, and M. Yu, "The design of miniaturized superconducting filters with the reflected group delay method," *IEEE Trans. Appl. Supercond.*, vol. 20, no. 4, pp. 2265–2271, Aug. 2010.
- [27] M. S. Sorkherizi, A. A. Kishk, and M. Saad, "High rejection stacked bandpass filter optimized by group delay response," in *2015 IEEE MTT-S Int. Microw. Symp.*, May 2015, pp. 1–4.
- [28] X. Fan, S. Li, P. D. Laforge, and Q. S. Cheng, "A sequentially coupled filter design approach using the reflected group delay method and the implicit space mapping technique," in *2017 IEEE MTT-S Int. Microw. Symp. (IMS)*, June 2017, pp. 364–367.
- [29] A. A. San-Blas, J. Pérez-Guijarro, V. E. Boria, and M. Guglielmi, "Systematic procedure for the efficient design of folded waveguide comb-line filters," in *2019 IEEE MTT-S Int. Conf. Numer. Electromagn. Multiphys. Model. Optim. (NEMO)*, May 2019, pp. 1–4.
- [30] A. A. San-Blas, A. Coves, A. Vidal, and V. E. Boria, "Efficient design of compact H-plane rectangular waveguide band-pass filters with integrated coaxial excitation," *AEU-Int. J. Electron. Commun.*, vol. 135, p. 153744, Apr. 2021.
- [31] J. W. Bandler, R. M. Biernacki, S. H. Chen, R. H. Hemmers, and K. Madson, "Electromagnetic optimization exploiting aggressive space mapping," *IEEE Trans. Microw. Theory Techn.*, vol. 43, no. 12, pp. 2874–2882, Dec. 1995.
- [32] Á. A. San-Blas, M. Guglielmi, J. C. Melgarejo, Á. Coves, and V. E. Boria, "Design procedure for bandpass filters based on integrated coaxial and rectangular waveguide resonators," *IEEE Trans. Microw. Theory Techn.*, vol. 68, no. 10, pp. 4390–4404, Oct. 2020.
- [33] J.-S. Hong and M. J. Lancaster, *Microstrip Filters for RF/Microwave Applications*. Hoboken, NJ, USA: Wiley, 2001.
- [34] G. Conciauro, M. Guglielmi, and R. Sorrentino, *Advanced Modal Analysis*. Hoboken, NJ, USA: Wiley, 2000.



HOJJAT JAMSHIDI-ZARMEHRI was born in Torbat-e-Heydarieh, Iran, in 1990. He received the B.Sc. degree in electrical engineering from the University of Birjand, Birjand, Iran, in 2012, and the M.Sc. degree in electrical engineering from Ferdowsi University of Mashhad, Mashhad, Iran, in 2018. His research interests include design and development of microwave bandpass filters, antenna design, and wave propagation.



ÁNGEL A. SAN-BLAS was born in Fortaleny, Valencia, Spain. He received the M.Sc. and Ph.D. degrees in telecommunications engineering from the Universitat Politècnica de València (UPV), Valencia, Spain, in 2000 and 2008, respectively.

From 2001 to 2002, he was a Researcher Assistant with the Departament de Comunicacions, UPV, where he was involved in the development of simulation tools for the analysis and design of waveguide devices. From November 2001 to March 2002, he was a Researcher with the Department of Electronics, Università degli Studi di Pavia, Pavia, Italy, where he was involved in the research project Millimeter-Wave and Microwave Components Design Framework for Ground and Space Multimedia Network (V European Framework Project). Since 2003, he has been an Associate Professor with the Department of Communications Engineering, Miguel Hernández University of Elche, Elche, Spain. His current research interests include the analysis and design of passive waveguide components for satellite communication systems.



MOHAMMAD H. NESHATI (Senior Member, IEEE) was born in Yazd, Iran. He received his B.Sc. degree in electrical engineering from Isfahan University of Technology, Isfahan, Iran, the M.Sc. degree from Amir-Kabir University of Technology, Tehran, Iran, and a Ph.D. degree from the University of Manchester (UMIST), Manchester, U.K.

Since 2006, he has been with the Department of Electrical Engineering of the Ferdowsi University of Mashhad, Iran, where he is an Associate Professor. He is a senior member of IEEE and also a member of the Antennas and Propagation Society (IEEE AP-S) and Microwave Theory and Techniques Society (IEEE MTT-S). His current research works include electromagnetic theory, antenna theory and design, and microwave active and passive circuit design.

Dr. Neshati is also a member of the Editorial Board of some journals, including the International Journal of Electronics and Communications, AEUE, the International Journal of RF and Microwave Computer-Aided Engineering and the International Journal of Antennas and Propagation.



SANTIAGO COGOLLOS (Member, IEEE) was born in Valencia, Spain, in 1972. He received the “Ingeniero Superior de Telecomunicación” and “Doctor Ingeniero de Telecomunicación” degrees from the Universitat Politècnica de València (UPV), Valencia, Spain, in 1996 and 2002, respectively.

In 2000, he joined the Communications Department of the UPV, where he was an Assistant Lecturer from 2000 to 2001, a Lecturer from 2001 to 2002, Associate Professor from 2002 to 2022, and became Full Professor in 2022. He has collaborated with the European Space Research and Technology Centre of the European Space Agency in the development of modal analysis tools for payload systems in satellites. In 2005, he held a post-doctoral research position working in the area of new synthesis techniques in filter design at University of Waterloo, Waterloo, Ont., Canada. His current research interests include applied electromagnetics, mathematical methods for electromagnetic theory, analytical and numerical methods for the analysis of microwave structures, and design of waveguide components for space applications.



ABHISHEK SHARMA was born in New Delhi, India, in 1992. He obtained his Bachelor's degree in Electronics and Communication at the Technical University of Uttar Pradesh, India, in 2014, and his Master's degree in Microwave and Optical Communication at the Department of Electronics and Communication of Delhi Technological University, India, in 2017.

During 2017-2019, he worked as an RF design engineer in the Microwave Component Division of Bharat Electronics Limited, under the Ministry of Defence of India, where he participated in the design of TR modules for active phased arrays and radars. In 2019, he started his doctoral studies at the Microwave Applications Group of the Universitat Politècnica de València, Spain, as an Early Stage Researcher of the TESLA Network. During his Ph.D., he developed novel compact solutions for reconfigurable waveguide filters and multiplexers. His research interest includes high-power filter design, reconfigurable filters, transmit-receive modules, RF subsystems and radars.



VICENTE E. BORIA (Fellow, IEEE) was born in Valencia, Spain, on May 18, 1970. He received his “Ingeniero de Telecomunicación” degree (with first-class honors) and the “Doctor Ingeniero de Telecomunicación” degree from the Universidad Politècnica de València (UPV), Valencia, Spain, in 1993 and 1997, respectively.

In 1993 he joined the “Departamento de Comunicaciones”, UPV, where he has been Full Professor since 2003. In 1995 and 1996, he was holding a Spanish Trainee position with the European Space Research and Technology Centre, European Space Agency (ESTEC-ESA), Noordwijk, The Netherlands, where he was involved in the area of EM analysis and design of passive waveguide devices. He has authored or co-authored 15 chapters in technical textbooks, 200 papers in refereed international technical journals, and over 250 papers in international conference proceedings. His current research interests are focused on the analysis and automated design of passive components (in particular filters and multiplexers) in several technologies, as well as on the simulation and measurement of power effects in high-frequency devices and systems.

Dr. Boria has been a member of the IEEE Microwave Theory and Techniques Society (IEEE MTT-S) and the IEEE Antennas and Propagation Society (IEEE AP-S) since 1992. He is also member of the European Microwave Association (EuMA), and has been the Chair of the 48th European Microwave Conference held in Madrid, Spain. He acts as a regular reviewer of the most relevant IEEE and IET technical journals on his areas of interest. He has been Associate Editor of IEEE Microwave and Wireless Components Letters (2013-2018) and IET Electronics Letters (2015-2018). He currently serves as Subject Editor (Microwaves) of IET Electronics Letters, and as Editorial Board member of International Journal of RF and Microwave Computer-Aided Engineering. He is also member of the Technical Committees of the IEEE-MTT International Microwave Symposium and of the European Microwave Conference.



ÁNGELA COVES (Senior Member, IEEE) received the Licenciado and Ph.D. degrees in physics from the University of Valencia, Spain, in 1999 and 2004, respectively. She is currently a Professor with the Department of Communications Engineering, Miguel Hernández University of Elche, Elche, Spain. Her research interests include microwave passive components, RF breakdown high-power effects, and waveguide theory.

...